

# Developing multiple-site kinetic models in catalysis simulation: A case study of $\text{O}_2 + 2\text{NO} \leftrightarrow 2\text{NO}_2$ oxidation–reduction chemistry on Pt(100) catalyst crystal facets

R.S. Disselkamp\*, R.G. Tonkyn, Ya-Huei Chin, C.H.F. Peden

*Institute for Interfacial Catalysis, Pacific Northwest National Laboratory, 3335 Q Avenue, P.O. Box 999, MS K8-93, Richland, WA 99352, USA*

Received 17 May 2005; revised 9 November 2005; accepted 22 November 2005

Available online 22 December 2005

## Abstract

It is generally recognized that developing a kinetic model for a supported catalyst is difficult because of the existence of multiple sites. These sites can arise from a distribution of crystal facets (e.g., (100), (110)) each with its unique intrinsic site types (e.g., atop, bridge, hollow). Additional complexities arise from non-basal plane site types (e.g., defect, edge, corner), the differing lateral interaction energies of which may be coverage-dependent for each of their pairwise interactions. To demonstrate the complexities that develop for even a greatly simplified system, we examine a multiple site kinetic model of the reaction  $2\text{NO} + \text{O}_2 \leftrightarrow 2\text{NO}_2$  on an ideal Pt(100) catalyst. A model of the Pt(100) surface is adopted where atop, bridge, and fourfold hollow sites are responsible for  $\text{O}_2$ , NO, and  $\text{NO}_2$  chemisorption to form Pt–O, Pt–NO, and Pt– $\text{NO}_2$  species. In our kinetic scheme, equilibrium is assumed for  $\text{O}_2$ , NO, and  $\text{NO}_2$  chemisorption due to their high sticking coefficients (all  $>0.1$ ). A single rate-determining step of the Langmuir–Hinshelwood type was chosen to describe the oxidation of NO on platinum via the reaction  $\text{Pt}_{\text{H,A,B}}\text{–O} + \text{Pt}_{\text{H,A,B}}\text{–NO} \leftrightarrow \text{Pt}_{\text{H,A,B}} + \text{Pt}_{\text{H,A,B}}\text{–NO}_2$ , where H, A, and B represent hollow, atop, and bridge sites. Equal kinetic parameters for all site combinations were assumed to exist and were in part taken from the literature to be  $\Delta H^\ddagger = 83 \text{ kJ/mol}$  and  $\Delta S^\ddagger = 20 \text{ J/(K mol)}$ . The exercise here is largely hypothetical but offers insight into how more detailed kinetic models may be developed, such as through the use of reaction velocity matrices, a concept introduced here. Specifically for this system, the model yielded insight into  $\text{NO}_x$  chemistry on Pt(100) in that it predicted that the greatest reaction velocities (forward and reverse) occurred via the reaction  $\text{Pt–O(atop)} + \text{Pt–NO(bridge)} \leftrightarrow \text{Pt(atop)} + \text{Pt–NO}_2(\text{bridge})$ . We believe that the framework of a site-specific modeling scheme presented here is an important starting point for future site-specific microkinetic modeling. In particular, a definition and description of use of surface coverages, reaction rate coefficients, and computed reaction velocity matrices are presented.

© 2005 Elsevier Inc. All rights reserved.

**Keywords:** Multiple-site kinetic model; Site-specific microkinetic modeling

## 1. Introduction

It is generally agreed that supported catalysts are complex in that they can have distributions of crystal facets (e.g., (100), (110), (111)), each with unique site types (e.g., atop, bridge, hollow), in addition to defect, edge, and corner entities available for adsorption and reaction. In principle, each of these microscopic site types has unique reaction kinetic parameters, which are made even less tractable by lateral site type (and perhaps

modeled by pairwise) interactions. It can be argued that even detailed microkinetic models, where in principle all elementary reactions for a process are considered, are only approximations of the true system and may have insufficient predictive capabilities. This is because typically for each elementary reaction, only a single enthalpy and entropy of activation for the reaction cannot be expected to be universally valid for a wide range of temperature, pressure, and composition in a system comprising an ensemble of microscopic site types.

As a case study in model development, here we examine a highly simplified multiple-site kinetic model of the reaction  $2\text{NO} + \text{O}_2 \leftrightarrow 2\text{NO}_2$  on an ideal Pt(100) catalyst compris-

\* Corresponding author. Fax: +509 376 5106.

E-mail address: [robert.disselkamp@pnl.gov](mailto:robert.disselkamp@pnl.gov) (R.S. Disselkamp).

ing only this crystal facet. The chemistry modeled here can be thought of as a subset of properties of an actual supported catalyst (e.g., Pt/Al<sub>2</sub>O<sub>3</sub>) that contains many more site types. The multiple-site model here is greatly simplified, and hence only hypothetical in nature, in that only a single rate-determining step (RDS) of the Langmuir–Hinshelwood type is assumed, together with assumed equilibrium gas adsorption. Despite the unrealistic nature of our model, however, we use it to demonstrate the complex nature of developing a multiple-site kinetic model for even a simple system. In doing so, we introduce the concept of (forward and reverse) site-specific reaction velocity matrices that are quantitative descriptions of molecular-level kinetic phenomena, and discuss their use and application to more general systems.

As a secondary issue, nitrogen oxides emitted from vehicles represent a major source of gasoline and diesel engine pollution. This has led to the development of NO<sub>x</sub> storage/reduction (NSR) catalysts whereby platinum is used to oxidize NO to NO<sub>2</sub> and the latter is stored during lean-burn conditions on Ba-containing materials [1–5]. Thus NO oxidation to NO<sub>2</sub> on platinum is a key process in NO<sub>x</sub> storage on BaO. Previous empirical kinetic models of NO oxidation have been developed for this purpose [6–9]. Most pertinent to our discussion here are the DFT computations by Neurock et al. [7,8] of site-specific chemisorption binding energies for NO, O<sub>2</sub>, and NO<sub>2</sub>, which we use in our modeling here. In their work, generic (site independent) kinetic parameters for reactions were used in the Monte Carlo kinetic algorithm.

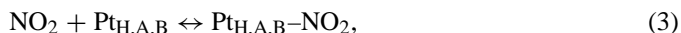
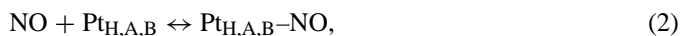
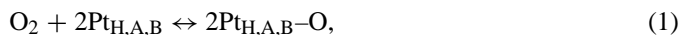
## 2. Results and discussion

### 2.1. The model

#### 2.1.1. Postulated kinetic model

To apply our multiple-site model of O<sub>2</sub> + 2NO ↔ 2NO<sub>2</sub> chemistry on a platinum catalyst, we assumed that chemistry occurs in a plug-flow reactor. The assumed reactor had an inside diameter of 2.0 cm, a total catalyst volume of 4.2 cm<sup>3</sup>, and a void fraction of ~0.6 and contained 70 μmol of platinum. A reactor temperature of 523 K and a gas flow rate of 1.0 SLPM were used. We also assumed an average Pt particle size of 22 Å, corresponding to 120 m<sup>2</sup>/g [10]. These assumptions led to an exposed Pt catalyst surface area density of 3900 cm<sup>2</sup>/cm<sup>3</sup>. The gas mix entering the reactor was taken to be 8.0% O<sub>2</sub>/500 ppm NO/~0 ppm NO<sub>2</sub>. Equal kinetic parameters for all site combinations (see below) were assumed to exist and were taken in part from the literature to be ΔH<sup>†</sup> = 83 kJ/mol [8] and ΔS<sup>†</sup> = 20 J/(K mol).

The modeling procedure used to obtain the reactor effluent NO and NO<sub>2</sub> concentrations was as follows. We assumed that NO oxidation on Pt(100) could be described using the following elementary reactions:



and



Here the subscripts A, B, and H represent atop, bridge, and four-fold hollow sites in our assumed Pt(100) surface [7,8]. A full justification of the chemistry occurring solely on the Pt(100) surface cannot be made. For example, the ratio of Pt(100) to Pt(111) (the more stable crystal facet) can be estimated using the procedure of Hardeveld and Hartog [11,12], assuming that the polycrystalline sample is cubo-octahedron in shape. From the assumed average platinum particle size of 22 Å, we estimate this ratio to be ~0.20. Similarly, based on comparable O<sub>2</sub> heats of adsorption on Pt(100) and Pt(111) facets (~–250 kJ/mol) [13], both facets may be important in NO oxidation. As discussed earlier, the purpose here is to provide a site-specific kinetic modeling framework for reaction schemes of more general interest.

It is possible that only a subset of the A, B, and H sites has a significant effect on the overall kinetics of these reactions. This will become clearer in the next section on equilibrium gas adsorption. The forms of reactions (1)–(3) are identical to those of the model by Olsson [6], with the important exception that we now treat gas adsorption on different sites separately. Chemistry is described by reaction (4), which has the form of a Langmuir–Hinshelwood bimolecular surface reaction, as discussed in detail previously [14]. The approach that we adopt here is to assume equilibrium for reactions (1)–(3) and consider reaction (4) to be the RDS.

Modeling simulations of plug-flow chemistry were computed by assuming that the chemistry occurs in 50 equal-volume axial elements. This was done by taking the output concentrations of each element as input concentrations to the next element. For each element, the input concentrations were used to compute surface coverages, and then these coverages were used to compute reaction velocities and, through a mass balance relation, modify effluent gas-phase concentrations.

#### 2.1.2. Equilibrium adsorption

An early experimental investigation illustrating multiple adsorption sites on platinum was a TPD study by Bartram [15] that determined additional surface site(s) exist for reversible NO<sub>2</sub> adsorption (with saturation at θ<sub>NO<sub>2</sub></sub> = 0.15 ML) after oxygen chemisorption on Pt(111) (via O<sub>2</sub>, with θ<sub>O</sub> = 0.75). That study was performed in conjunction with HREELS, which demonstrated a lack of NO<sub>3</sub> absorption spectroscopic features on NO<sub>2</sub> adsorption on the oxygen-covered Pt surface; thus the authors concluded that two distinct surface sites exist for adsorbed oxygen and NO<sub>2</sub>. The NO/NO<sub>2</sub> system on platinum was further studied experimentally using TPD and HREELS by that group [16,17] and others [18,19]. Insight into the site-specific nature of O<sub>2</sub> chemisorption enthalpy on platinum can be obtained by calorimetric [20,21] and DFT calculations [5,8]. It has been concluded from these DFT calculations that two distinct surface adsorption sites exist for chemisorbed oxygen on Pt(100). The DFT-computed adsorption enthalpies for O<sub>2</sub>, NO, and NO<sub>2</sub> at low surface coverage have been published by Mei [8], and we

Table 1  
Enthalpies of chemisorption for O<sub>2</sub>, NO and NO<sub>2</sub> on the Pt(100) surface<sup>a</sup>

	$\Delta H$ (kJ/mol)		
	O <sub>2</sub>	NO	NO <sub>2</sub>
Pt(100) atop	0.0	–136.0	–119.0
Bridge	–219.0	–214.0	–74.0
4-fold hollow	–149.0	–158.0	0.0

<sup>a</sup> Taken from Ref. [8].

Table 2  
Representative calculated adsorption free energies and surface coverage at 523 K using the thermodynamic data of Table 1

	O <sub>2</sub>	NO	NO <sub>2</sub>	Empty
$\Delta S$ (J/(K mol))	–34.7	–161.0	–163.0	
$\Theta(\text{Pt-X})^a$				
Atop	$4.2 \times 10^{-3}$	$4.4 \times 10^{-10}$	$1.7 \times 10^{-10}$	0.996
Bridge	0.997	$3.4 \times 10^{-3}$	$6.3 \times 10^{-13}$	$6.6 \times 10^{-6}$
Hollow	0.767	$2.9 \times 10^{-10}$	$1.7 \times 10^{-13}$	0.234

<sup>a</sup>  $\Theta$  denotes a fractional surface coverage compared to saturation ( $\Theta = 1$ , see text), with X = O, NO, NO<sub>2</sub>, or empty (vacant) site identity.

used these in our model; see Table 1. In this table we assigned a zero enthalpy of adsorption for Pt<sub>A</sub>–O and Pt<sub>H</sub>–NO<sub>2</sub> species, because these species were determined to be nonbonding, and these zero adsorption enthalpies do not introduce modeling error via their correspondingly small surface coverage values obtained (see Table 2).

We used our fitting algorithm to compute equilibrium surface concentrations arising from O<sub>2</sub>, NO, and NO<sub>2</sub> chemisorption as follows. For each given NO and NO<sub>2</sub> (and invariant O<sub>2</sub>) concentration, a site coverage 3 × 4 matrix was determined for atop, bridge, and fourfold hollow sites that could be populated by Pt–O, Pt–NO, Pt–NO<sub>2</sub>, and Pt (empty or unoccupied) moieties. This site-specific coverage matrix was obtained through an iterative procedure by first guessing at  $\Theta_A$ ,  $\Theta_B$ , and  $\Theta_H$  site coverages (i.e., fractional occupation by summed Pt–O, Pt–NO, or Pt–NO<sub>2</sub> occupation) and then computing enthalpies and entropies of chemisorption. The enthalpies for NO and NO<sub>2</sub> are given by the following expressions:

$$\Delta H_{A,i} = \Delta H_{A,i}^0 [1 - 0.8\Theta_B], \quad (5a)$$

$$\Delta H_{B,i} = \Delta H_{B,i}^0 [1 - 0.4(\Theta_B + \Theta_H)], \quad (5b)$$

and

$$\Delta H_{H,i} = \Delta H_{H,i}^0 [1 - 0.8\Theta_B], \quad (5c)$$

where  $i = \text{NO or NO}_2$  and the right-side standard-state enthalpies are the low-coverage values given in Table 1. Similarly, for O<sub>2</sub>, we used the following expressions:

$$\Delta H_{A,O_2} = \Delta H_{A,O_2}^0 [1 - 0.8\Theta_A\Theta_B], \quad (6a)$$

$$\Delta H_{B,O_2} = \Delta H_{B,O_2}^0 [1 - 0.4(\Theta_A\Theta_B + \Theta_B\Theta_H)], \quad (6b)$$

and

$$\Delta H_{H,O_2} = \Delta H_{H,O_2}^0 [1 - 0.8\Theta_B\Theta_H]. \quad (6c)$$

The factor of 0.8 (or 0.4) arises from the DFT-estimated adsorption enthalpy reduction arising from increasing surface coverage [8]. With these enthalpies specified together with entropies (see below), the free energy of chemisorption,  $\Delta G_{\text{ad}} = \Delta H_{\text{ad}} - T\Delta S_{\text{ad}}$  were computed at the appropriate temperature. Next, the surface coverage ratios were determined from the equilibrium constants,  $K_{\text{ad}} = \exp(-\Delta G_{\text{ad}}/RT)$ , where  $K_{\text{ad}} = [(\text{PtX}/\text{Pt})^n/P_X]$  with X = O, NO, and NO<sub>2</sub> and  $n = 2, 1$ , and 1, respectively, and  $P_X$  is the appropriate gas partial pressure of O<sub>2</sub>, NO, or NO<sub>2</sub> (atm). Finally these surface site-specific coverages were used to calculate  $\Theta_A$ ,  $\Theta_B$ , and  $\Theta_H$ , and these values were compared with the originally guessed values and the error between guessed and computed was minimized numerically. This numerically intensive process was repeated for all NO and NO<sub>2</sub> concentrations for each axial slice of the plug-flow reactor.

We now address the method for estimating adsorption entropies in our calculations. Unfortunately, no previously published values of adsorption entropy exist for our system. There are many ways to approximate adsorption entropy, however, and it is fortunate that the various methods agree well when adjusted to standard-state conditions. For example, Trouton's rule states that the entropy of vaporization of a liquid is 85 J/(K mol) [22], which may have similar condensed phase-to-gas phase ratios of molecular partition functions as our system reported here. Indeed, a recent study by Sellers [23] that determined adsorbate-to-gas phase desorption entropies from TPD data of 15 chemisorption and physisorption systems assigned an entropy of  $91 \pm 14$  J/(K mol) (95% confidence interval) for all data examined. All of these systems were for nondissociative adsorption; we need to take a different approach for O<sub>2</sub> chemisorption here.

First, however, if it is assumed that on surface chemisorption of nondissociative adsorption (e.g., both NO and NO<sub>2</sub>), a reduction in the translational degrees of freedom from 3 to 2 and a gain of 1 vibrational (adsorbate) degree of freedom occur, then, as shown by Eichler and Zvara [24], the adsorption entropy change (for a two-dimensional gas) can be written as

$$\Delta S_{\text{ad}} = R \ln \left[ \left( \frac{h^2}{2\pi mkT} \right)^{1/2} \frac{A}{V} \frac{e^{-hv/2kT}}{(1 - e^{-(hv/kT)})} \right], \quad (7)$$

where  $m$  is the mass of NO (or NO<sub>2</sub>),  $T$  is temperature (K), and  $\nu$  is the adsorbate surface vibrational frequency ( $\sim 500$  cm<sup>–1</sup> is assumed [25]). The quantity  $A/V$  is the area per surface site divided by volume per gas phase molecule undergoing adsorption. Our procedure for estimating  $A/V$  is somewhat different than that of Goss [26] and Eichler and Zvara [24], who used differing standard-state  $A/V$  quantities. Here we took  $A$  to be the area per absorption site ( $8.0 \times 10^{-20}$  m<sup>2</sup>/site [6]), and  $V$  to be the volume per gas-phase molecule computed from gas-phase concentrations. Similarly, for O<sub>2</sub> dissociative chemisorption, the entropy change can be envisioned as the loss of the diatomic vibrational degree of freedom of O<sub>2</sub> (1555 cm<sup>–1</sup> [27]), a loss of one gas phase, and a gain of 2 surface translational degrees of freedom (from dissociation). Thus the adsorption entropy change for oxygen chemisorption can be approximated by the following expression using standard translational and vibra-

tional partition function information [24,28]:

$$\Delta S_{\text{ad}} = R \ln \left[ \left( \frac{2\pi mkT}{h^2} \right)^{1/2} \frac{A^2}{V} \frac{e^{-hv(s)/kT}}{(1 - e^{-(hv(s)/kT)})^2} \times \frac{(1 - e^{-hv(g)/kT})}{e^{-hv(g)/2kT}} \right]. \quad (8)$$

The adsorption entropies computed from Eqs. (7) and (8) have only weak temperature dependence. Table 2 lists the adsorption entropies computed at 523 K. Although at first inspection it appears that the adsorption entropy for NO and NO<sub>2</sub> are somewhat large, when corrected for standard state conditions (via  $\Delta S_{\text{correction}} = R \ln(P/P^0)$ ), an average NO and NO<sub>2</sub> value of the standard state entropy of  $\Delta S^0 = 88 \text{ J/(K mol)}$  is obtained. This value is close to the values obtained by Sellers [23] based on TPD data, and also to the value of 85 J/K from Trouton's rule discussed earlier. It is also noteworthy that the adsorption entropy for O<sub>2</sub> is smaller (less negative) than that for NO and NO<sub>2</sub>, as expected because it undergoes dissociative chemisorption.

To illustrate the expected surface coverage of O<sub>2</sub>, NO, and NO<sub>2</sub> on Pt(100) under typical conditions, we chose a representative temperature (523 K) and computed adsorption surface coverage matrix results for the atop, bridge, and fourfold hollow sites. Again, the relevant adsorption entropies are given in Table 2, with the  $3 \times 4$  coverage matrix provided at the bottom of this table. It is seen that O<sub>2</sub> was bound almost exclusively to the bridge and hollow sites with near-saturation coverage. Conversely, the saturation surface coverage of NO was small, with the greatest coverage on the bridge site (e.g.,  $\Theta_B = 3.4 \times 10^{-3}$ ). Somewhat surprisingly, a much smaller coverage of NO<sub>2</sub> for all sites was seen, with the largest value of  $\Theta_A = 1.7 \times 10^{-10}$  on the atop site. This suggests, based on the population of surface sites only, that NO<sub>2</sub> reduction (reverse of rxn (4)) may be greatest when Pt–NO<sub>2</sub>(atop) reacts with Pt(atop). Similarly, NO oxidation may be more favorable when NO is bound on a bridge site reacting with Pt–O(bridge or hollow).

### 2.1.3. Kinetic considerations

The Langmuir–Hinshelwood reaction velocity (molecules/(cm<sup>3</sup> s)) corresponding to reaction (4) can be written as [14]

$$v_{X-Y}(4) = \frac{kT}{2h} z_{X-Y}(\chi/L) \exp(\Delta S^\ddagger/R) \times \exp(-\Delta H^\ddagger/RT) \Theta_X \Theta_Y, \quad (9)$$

where  $z_{X-Y}$  is the number of nearest-neighbor X–Y site pairs per unit cell,  $L$  is the Pt(100) unit cell number surface density ( $8.0 \times 10^{-16} \text{ cm}^{-2}$  [29]),  $\chi$  is the surface area density of the active catalyst ( $3900 \text{ cm}^2/\text{cm}^3$ ),  $\Delta H^\ddagger$  and  $\Delta S$  represent the enthalpy and entropy of activation (e.g., to the transition state), and  $\Theta_X$  and  $\Theta_Y$  represent the (fractional) surface coverage, as discussed in the previous section. Here X and Y are all permutations of atop, bridge, and hollow sites, with a total of nine forward and nine reverse reactions possible. Inspection of the unit cell facilitates evaluation of the values of  $z_{X-Y}$ ; the values of  $z$  are presented in Table 3.

Table 3

Site-specific reaction enthalpies for Pt–O + Pt–NO → Pt + Pt–NO<sub>2</sub> (i.e., reaction (4))<sup>a</sup>

Pt–O (↔ Pt)	Pt–NO (↔ Pt–NO <sub>2</sub> )	$\Delta H(\text{rxn (4)})$ (kJ/mol) forward/reverse	$z_{X-Y}$
Atop	Atop	102.8/157.8	4
Atop	Bridge	141.3/102.8	4
Atop	Hollow	102.8/129.6	4
Bridge	Atop	123.4/102.8	2
Bridge	Bridge	216.9/102.8	4
Bridge	Hollow	151.6/102.8	2
Hollow	Atop	102.8/128.9	4
Hollow	Bridge	170.2/102.8	2
Hollow	Hollow	104.9/102.8	0 <sup>b</sup>

<sup>a</sup> Based on values from Table 2 and thermodynamic restriction relation for reactions (1)–(4) and (10), see text.

<sup>b</sup> Hollow–hollow pairing distance is one unit cell dimension apart and hence taken to be zero.

For our kinetic simulation, we used thermodynamic restriction in our analysis [14]. We did this using a reaction enthalpy of  $-58.4 \text{ kJ/mol}$  at our midpoint temperature of 550 K [30] for the following reaction:



Thus, we used the following relation for our site-specific reaction enthalpies:

$$\Delta H(\text{rxn (4)}) = \Delta H(\text{rxn (10)}) + \Delta H(\text{rxn (3)}) - (1/2)\Delta H(\text{rxn (1)}) - \Delta H(\text{rxn (2)}), \quad (11)$$

where the right side gives known site-specific quantities. As mentioned earlier, we used a single enthalpy and entropy of activation in our simulation. This was done only for the sake of convenience, to reduce the number of parameters to fit. In principle, it is reasonable to expect that different permutations of sites would have unique reaction energies. As we discuss later, however, because we identified a single-site X–Y pair as being responsible for >85% of the reaction velocity, it is plausible to suspect that only a single enthalpy and entropy of activation in our modeling need be fit.

## 2.2. Simulation of plug-flow reactor chemistry

Our modeling used a Fortran program with combinatorial minimization (i.e., simulated annealing) according to the method and computer code of Goffe et al. [31]. Function minimization was needed to solve for the equilibrium surface concentrations at each of the 50 axial “slices” of the reactor volume. The linear first-order differential equation solving routine LSODES [32,33] was used to simulate reaction (4) and hence modify the gas-phase NO and NO<sub>2</sub> concentrations along the plug-flow reactor.

Arguably one of the most useful predictions made by the model is the predicted reaction velocities for all permutations of surface sites. We computed, according to rxn (9), both a forward and reverse  $3 \times 3$  reaction velocity matrix. For example, the forward rxn (9) matrix consisted of Pt–O versus Pt–NO velocities for atop, bridge, and hollow sites. Inspecting these matrices,



Table 4

Forward and reverse reaction velocity matrices at reactor outlet are given (505 K, mol/(cm<sup>2</sup> s)). Here 500 ppm of NO<sub>2</sub> and no NO was input into the reactor

Forward	NO-atop	NO-bridge	NO-hollow
O-atop	$1.5 \times 10^{13}$	$1.7 \times 10^{16}$	$9.5 \times 10^{12}$
O-bridge	$1.5 \times 10^{13}$	$1.1 \times 10^{11}$	$1.5 \times 10^{10}$
O-hollow	$2.7 \times 10^{15}$	$1.9 \times 10^{15}$	0.0
Reverse	NO <sub>2</sub> -atop	NO <sub>2</sub> -bridge	NO <sub>2</sub> -hollow
Empty-atop	$4.4 \times 10^9$	$4.9 \times 10^{12}$	$2.8 \times 10^9$
Empty-bridge	$4.5 \times 10^9$	$3.2 \times 10^7$	$4.4 \times 10^6$
Empty-hollow	$7.9 \times 10^{11}$	$5.7 \times 10^{11}$	0.0

given in Table 4, reveals that for both the forward and reverse rxn (4) processes, atop-bridge combinations contributed ~80% to the total velocity for Pt-O(atop) + Pt-NO(bridge) ↔ Pt(atop) + Pt-NO<sub>2</sub>(bridge). This is somewhat surprising for the reverse velocity; according to Table 2, a prediction based on surface coverage alone would imply that the Pt-NO<sub>2</sub>(atop) + Pt(atop) combination would have had a greater velocity. Indeed, this was only 0.1% of the total reaction velocity.

### 3. Conclusion

In this work we have presented a site-specific model of NO<sub>x</sub> chemistry on an ideal Pt(100) catalyst. We have also introduced the concept of reaction velocity matrices, which can be obtained from site-specific reaction rate parameters ( $\Delta H^\ddagger$  and  $\Delta S$ ) and site-specific surface coverage matrices. For example, an  $A \times B$  reaction velocity matrix (e.g.,  $R_{A,B}$ ) is defined here to have  $A$  = number of distinct site types and  $B$  = number of chemically unique species. In tensor form, this can be written as

$$R_{A,B} = \sum_C \sum_D (k_{A,B,C,D} \Theta_{A,B} \Theta_{C,D}), \quad (12)$$

where  $k_{A,B,C,D}$  is the pairwise site-specific Langmuir-Hinshelwood reaction rate coefficient term (four-dimensional) and  $\Theta_{A,B} \Theta_{C,D}$  is the site-specific surface coverage product. The four-dimensional rate coefficient term arises from the squared dependence of the (two-dimensional) site-specific surface coverage term (e.g., pairwise interaction of site-specific chemical entities).

There is both a forward and reverse reaction velocity matrix for a set of elementary reactions. The modeling result that computed reaction velocities are not completely correlated with surface coverage suggests that site-specificity is a necessity in microkinetic models of the future. This may be realized, in part, from accurate calculations of structure (e.g., binding energies, competitive vs. noncompetitive adsorption), as well as entropies and enthalpies of both (equilibrium) adsorption and (kinetic) activation processes.

### Acknowledgments

Financial support was provided by from the U.S. Department of Energy (DOE), Office of FreedomCar and Vehicle Technologies. This work was performed in the Environmental Molecu-

lar Sciences Laboratory (EMSL) at Pacific Northwest National Laboratory (PNNL). The EMSL is a national scientific user facility and supported by the U.S. DOE's Office of Biological and Environmental Research. PNNL is a multiprogram national laboratory operated for the U.S. DoE by the Battelle Memorial Institute (contract DE-AC06-76RLO 1830).

### References

- [1] N. Cant, M. Patterson, *Catal. Today* 73 (2002) 271.
- [2] S. Hodjati, C. Petit, V. Pitchon, A. Kiennenmann, *Appl. Catal. B: Environ.* 27 (2000) 117.
- [3] W.S. Epling, J.E. Parks, G.C. Campbell, A. Yezerets, N.W. Currier, L.E. Campbell, *Catal. Today* 96 (2004) 21.
- [4] P. Broqvist, I. Panas, E. Fridell, H. Persson, *J. Phys. Chem. B* 106 (2002) 137.
- [5] A. Eichler, J. Hafner, *J. Catal.* 204 (2001) 118.
- [6] L. Olsson, H. Persson, E. Fridell, M. Skoglundh, B. Andersson, *J. Phys. Chem. B* 105 (2001) 6895.
- [7] L.D. Kieken, M. Neurock, D. Mei, *J. Phys. Chem. B* 109 (2005) 2234.
- [8] D. Mei, Q. Ge, M. Neurock, L. Kieken, J. Lerou, *Mol. Phys.* 102 (4) (2004) 361.
- [9] L. Olsson, B. Westerberg, H. Persson, E. Fridell, M. Skoglundh, B. Andersson, *J. Phys. Chem. B* 103 (1999) 10433.
- [10] G. Ertl, H. Knozinger, J. Weitkamp (Eds.), *Handbook Heterogeneous Chemistry*, vol. 2, Wiley-VCH, New York, 1997, p. 441.
- [11] R. van Harveld, F. Hartog, *Surf. Sci.* 15 (1969) 189.
- [12] J.R. Anderson, *Structure of Metallic Catalysts*, Academic Press, New York, 1975.
- [13] G.A. Somorjai, *Introduction to Surface Chemistry and Catalysis*, Wiley, New York, 1994.
- [14] M. Boudart, G. Djega-Mariadassou, *Kinetics of Heterogeneous Catalytic Reactions*, Princeton University Press, Princeton, NJ, 1984.
- [15] M.E. Bartram, R.G. Windham, B.E. Koel, *Langmuir* 4 (1988) 240.
- [16] M.E. Bartram, R.G. Windham, B.E. Koel, *Surf. Sci.* 104 (1987) 57.
- [17] D.T. Wickham, B.A. Banse, B.E. Koel, *Surf. Sci.* 223 (1989) 82.
- [18] U. Schwalke, H. Niehus, G. Comsa, *Surf. Sci.* 152/153 (1985) 596.
- [19] W. Huang, Z. Jiang, J. Jiao, D. Tan, R. Zhai, X. Bao, *Surf. Sci.* 506 (2002) L287.
- [20] C.-B. Wang, C.-T. Yeh, *Appl. Catal. A: Gen.* 506 (2001) 1.
- [21] C.-B. Wang, H.-K. Lin, S.-N. Hsu, T.-H. Huang, H.-C. Chiu, *J. Mol. Catal. A: Chem.* 188 (2002) 201.
- [22] D.W. Oxtoby, H.P. Gillis, N.H. Nachtrieb, *Principles of Modern Chemistry*, fourth ed., Harcourt Brace Publ. Co., New York, 1999.
- [23] H. Sellers, *J. Phys. Chem. B* 107 (2003) 10206.
- [24] B. Eichler, I. Zvara, *Radiochim. Acta* 30 (1982) 233.
- [25] T. Jacob, R.P. Muller, W.A. Goddard III, *J. Phys. Chem. B* 107 (2003) 9465.
- [26] K.-U. Goss, *Environ. Sci. Technol.* 31 (1997) 3600.
- [27] D.A. McQuarrie, *Quantum Chemistry*, University Science Books, Mill Valley, CA, 1983.
- [28] D.A. McQuarrie, *Statistical Mechanics*, Harper & Row Publ. Co., New York, 1976.
- [29] J.R. Anderson, *Structure of Metallic Catalysts*, Academic Press, London, 1975.
- [30] Thermodynamics Research Center, NIST Boulder Laboratories Thermodynamics Source Database, in: M. Frenkel, P.J. Linstrom, W.G. Mallard (Eds.), *NIST Chemistry WebBook*, NIST Standard Reference Database Number 69, March 2003, National Institute of Standards and Technology, Gaithersburg, MD, 2003, p. 20899, <http://webbook.nist.gov>.
- [31] W.L. Goffe, G.D. Ferrier, J. Rogers, *J. Econometrics* 69 (1/2) (1994) 65.
- [32] A.C. Hindmarsh, in: R.S. Stepleman (Ed.), *ODEPACK: A Systematized Collection of Ordinary Differential Equation Solvers*, in *Scientific Computing*, North-Holland, Amsterdam, 1983, pp. 55–64.
- [33] S.C. Eisenstat, M.C. Gursky, M.H. Schultz, A.H. Sherman, *Int. J. Num. Meth. Eng.* 18 (1982) 1145.